Optics & Laser Technology 182 (2025) 112117

Contents lists available at ScienceDirect

Optics and Laser Technology

journal homepage: www.elsevier.com/locate/optlastec

Full length article

Low threshold lasing of GaN-based vertical-cavity surface-emitting lasers with thin InGaN/GaN quantum well active region

Rongbin Xu [a,*], Keisei Shibata [b], Hidefumi Akiyama [b], Jiazhe Zhang [a], Leiying Ying [a], Baoping Zhang [a,c,*]

[a] Department of Microelectronics and Integrated Circuits, Optoelectronics Laboratory of Micro/nano-Optoelectronics, Xiamen University, Xiamen 361005, China
[b] Institute for Solid State Physics, The University of Tokyo, Kashiwa, Chiba 277–8581, Japan
[c] Institute of Nanoscience and Applications (INA), Southern University of Science and Technology (SUSTech), Shenzhen 518055, China

ARTICLE INFO

Keywords:
InGaN quantum wells
Thin well and barrier
Cavity effect
Vertical-cavity surface-emitting laser (VCSEL)

ABSTRACT

We studied the mechanism of low-threshold lasing of InGaN/GaN double quantum well (DQW) vertical-cavity surface-emitting lasers (VCSELs) showing a low threshold energy density of about 0.37mJ/cm^2 via optical pumping at room temperature (RT). The QW with thin well (2.5 nm) and barrier (6 nm) led to the stronger carrier localization effect and weaker quantum confined Stark effect (QCSE). Temperature-dependent photoluminescence (TDPL) and time-resolved photoluminescence (TRPL) were employed on half-cavity samples (VCSEL without top distributed Bragg reflector) to study the carrier dynamics in VCSEL microcavity. Compared with epitaxial layer, half-cavity samples showed the higher turning point temperature of TDPL peak energy, and the carrier lifetime measured by TRPL was shorter. The experimental results suggest that the stronger localization effect of thin QW and the strong coupling of QW and internal optical field can contribute to the low-threshold lasing of GaN-based VCSELs.

1. Introduction

In the past 20 years, III-nitride compound semiconductors have become part of our daily life, as they are already being commercially applied in many areas such as solid state lighting, full-color display, and optical storage. Owing to the well confinement of carriers, 2-dimension InGaN/GaN quantum wells (QWs) are widely used as the active layers in light emitting diodes (LEDs) and laser diodes (LDs) [1]. The thickness of well and barrier, which will affect the piezoelectric field, carrier transport and distribution, and excition localization in active layer, play a crucial role in the optical qualities of InGaN/GaN QWs [2–4]. The optical properties of InGaN/GaN QWs with different structures have been studied by a variety of optical techniques, including power-dependent photoluminescence (PDPL), temperature-dependent photoluminescence (TDPL), and time-resolved photoluminescence (TRPL), et al [5–8].

Recently, GaN-based photonic cavities have attracted widely attention because of their potential applications in microcavity light emitters such as microdisk [9,10], resonant cavity light emitting diode (RCLED) [11,12], vertical-cavity surface-emitting laser (VCSEL) [13–15], et al. When the light emitting medium is placed inside a cavity, the spontaneous emission rate can be boosted, which is known as cavity effect [16]. Due to the cavity effect, microcavity light emitters based on InGaN QW can exhibit special optical properties.

Many researches have focused on the impacts of InGaN QW on the edge emitting lasers, and draw the conclusion by numerical calculation [17,18]. However, compared to edge emitting lasers, VCSELs have shorter cavity length and stronger cavity effect. Once InGaN/GaN QWs are embedded in VCSEL optical microcavities, diagnosis of the InGaN/GaN QWs via PDPL, TDPL, TRPL becomes difficult since the cavity effects are too strong. Therefore, it is not easy to investigate internal physics such as gain generation of carriers at localized states [19] possibly contributing to low-threshold-lasing mechanism in InGaN/GaN QW VCSELs. We here solve this problem by studying half-cavity samples on a bottom distributed Bragg reflector (DBR) in addition to no-cavity samples (epi-layer samples without DBRs) and full-cavity samples (VCSEL samples with bottom and top DBRs).

In this work, we study mechanism of low-threshold lasing of InGaN/GaN double quantum well (DQW) VCSELs with thin well (2.5 nm) and barrier (6 nm) showing a low threshold energy density of about 0.37

* Corresponding authors.
E-mail addresses: xurongbin@xmu.edu.cn (R. Xu), bzhang@xmu.edu.cn (B. Zhang).

https://doi.org/10.1016/j.optlastec.2024.112117
Received 7 August 2024; Received in revised form 3 November 2024; Accepted 8 November 2024
Available online 14 November 2024

mJ/cm^2 via optical pumping at room temperature (RT). We prepared two samples having the same active layers of thin InGaN/GaN DQW without cavity and with a half-cavity for TDPL and TRPL measurements. In TDPL measurement, the two samples exhibited a typical S-shaped behavior (redshift–blueshift–redshift), while turning point temperature of peak energy increased for the sample with half-cavity. TRPL measurements show that the carrier lifetime for the sample with cavity decreases significantly, and at the fast decay stage, the carrier lifetime of high energy side is anomalously longer than that of low energy side. All these phenomena suggest that, in VCSEL microcavity, the transition of carrier in different QW localization states is inhibited, and the carrier capture efficiency of localization states can be enhanced due to the cavity-enhanced recombination. Since QWs with thin well and barrier show a stronger carrier localization effect, the strong coupling of QW and internal optical field can contribute to the low-threshold lasing of InGaN/GaN QW VCSEL.

2. Experimental methods

The epitaxial layers of the devices were grown on a c-plane (0001) sapphire substrate using metal organic chemical vapor deposition system. The active region consisted of two pairs of $In_{0.18}Ga_{0.82}N$ (2.5 nm)/ GaN (6 nm) QWs. The schematic diagram of epitaxial structure is shown in Fig. 1(a). This structure is identical to that of VCSEL fabricated and measured later. Fig. 1(c) show the schematic diagram of the fabricated VCSEL. To fabricate the device, 13.5-pairs TiO_2/SiO_2 were evaporated on the top of the grown VCSEL structure to form the bottom DBRs. Then, the structure was bonded onto a quartz substrate, followed by a laser lift-off (LLO) to remove the sapphire substrate. Next, the GaN surface was polished through chemical mechanical polishing (CMP) techniques. At this point, the sample with only bottom DBR (half-cavity structure) was achieved, as shown in Fig. 1(b). To ultimately achieve VCSEL, a top DBR with 12-pairs TiO_2/SiO_2 was deposited. The measured reflectivity of top and bottom DBR at the center wavelength of 440 nm are 99.97 % and 99.99 %, respectively. The detailed structure and material parameters of VCSEL are shown in Table 1.

Fig. 2 shows the excitation power-dependent normalized PL spectra of epitaxial layer and half-cavity structure at RT. In Fig. 2(a), the PL spectra of epitaxial layer exhibit a slight blueshift of the PL peak position together with the broadening of spectra linewidth at higher energy side. The line shape evolution and slight blueshift of the peak energy suggest that the effect of band-filling effect is much larger than the quantum confined Stark effect (QCSE). Therefore, we attribute the carrier emission behaviors and carrier lifetimes discussed later to the localization effect during the carrier transport and recombination processes in such an InGaN QW structure. For the half-cavity structure, the Fabry–Perot oscillations can be observed and the full width at half maximum (FWHM) of emission peak becomes narrow due to the cavity formed between bottom DBR and the top GaN/air interface, as shown in Fig. 2 (b).

3. Results and discussion

3.1. Optical properties measured by TDPL

The TDPL experiments were performed on epitaxial layer and half-

Table 1
Detailed layer structure of VCSEL.

Material	Thickness (nm)	Doping concentration (cm^{-3})	Refractive index
TiO_2/SiO_2 (12 pairs)	46/75	–	2.4/1.465
n-GaN	2280	$2.5x10^{18}$ (Si doped)	2.49
$In_{0.18}Ga_{0.82}N$/GaN	2 × 2.5/6	–	2.8/2.49
p-GaN	80	$4x10^{17}$ (Mg doped)	2.49
p-$Al_{0.18}Ga_{0.82}N$	20	$1x10^{18}$ (Mg doped)	2.45
p-GaN	600	$4x10^{17}$ (Mg doped)	2.49
SiO_2/ TiO_2 (13.5 pairs)	75/46	–	1.465/2.4

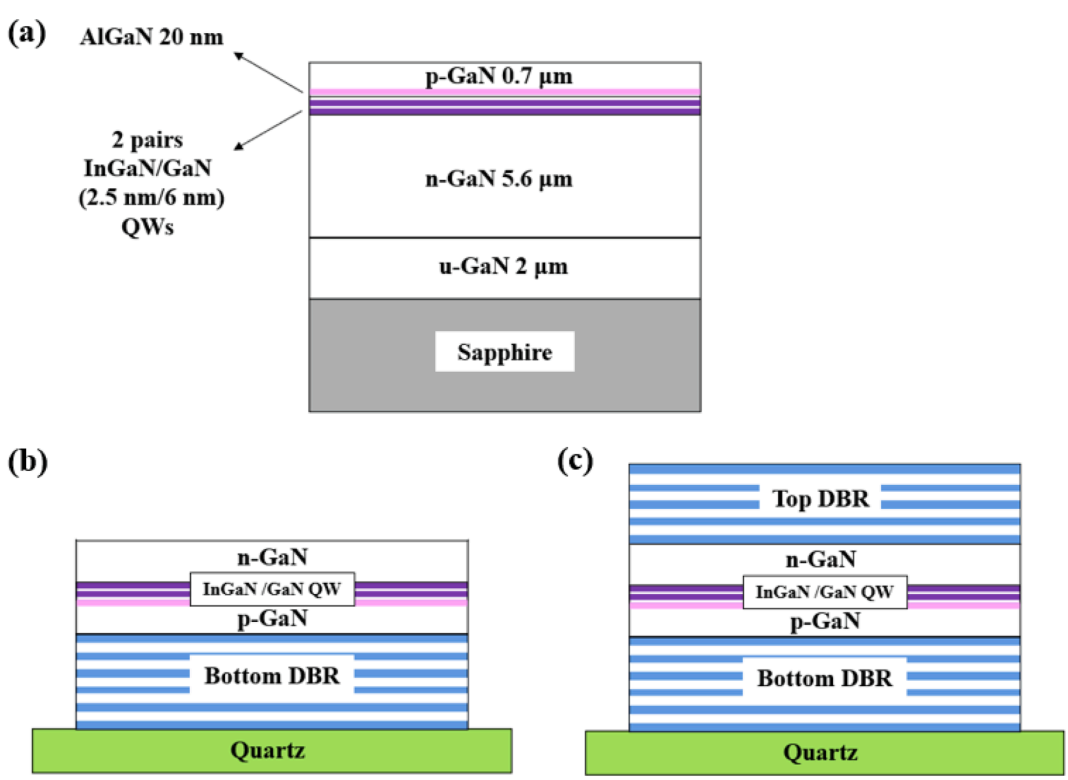

Fig. 1. Schematic diagram of (a) InGaN/GaN QW epitaxial layer, (b) half-cavity structure and (c) optical pumping GaN-based VCSEL.

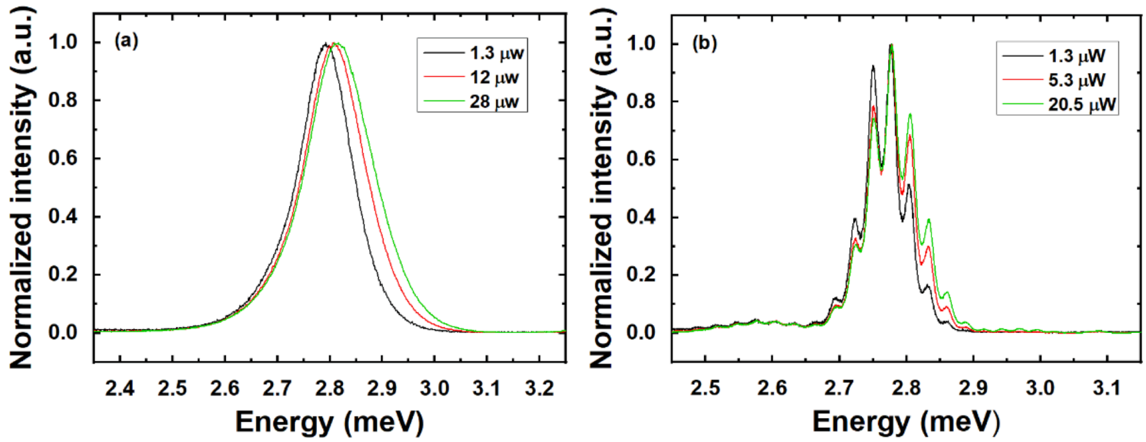

Fig. 2. Excitation power dependence of normalized PL spectra of (a) epitaxial layer and (b) half-cavity structure.

cavity structure over a temperature range of 15 to 300 K under excitation power of 1.3 μW. An internal quantum efficiency (IQE) of approximately 27.3 % is estimated by the ratio of integrated PL intensity at 300 K and that at 15 K. The relatively high IQE is attributed to the thin well and barrier in QWs, causing strong localization effect and weak QCSE. By fitting the PL spectra with a Gauss peak, the emission peak energy and FWHM are determined, as shown in Fig. 3. In Fig. 3(a), both peak energies show a "S shape" (redshift–blueshift–redshift) variation with increasing temperature. The variation of peak energy can be explained as the result of existence of different localization potential in QW structure: At low temperature, carriers are randomly distributed among the potential minimums. As the temperature is increased, the carriers localized weakly are thermally activated and relax down into the deeper localization potentials, which produces a redshift. By further increasing the temperature, the carriers may have sufficient energy to repopulate the shallow localized states, thus resulting in the blueshift of the peak energy. At even higher temperature, most carriers escape from the localized states and become free carriers. Then, a redshift of the peak energy is observed due to the temperature-induced bandgap shrinkage.

For half-cavity structure, both temperature of the turning point from redshift to blueshift (T = 50 K) and blueshift to redshift (T = 170 K) are found much higher than epitaxial layer (28 K and 130 K for turning point from redshift to blueshift and blueshift to redshift, respectively), which is believed to be relevant to the enhancement of radiative recombination rate due to the cavity effect. The higher temperature of first turning point suggests that the probability of thermally activated carriers relax down into the deeper localization potentials becomes smaller. And the higher temperature of second turning point suggests that the less probability of the carriers escape from the localized states to become free carriers. Therefore, the possible processes of carrier transport and relaxation in different localization potentials are prevented. A larger energy is needed for carriers to escape from the localization potential in half-cavity structure, and thus a higher temperature for turning point of peak energy.

Fig. 3(b) shows the TDPL linewidths. For epitaxial layer, the linewidth exhibits a slight reduction (5 to 23 K) followed by a linearly increase to 300 K. The slight reduction of linewidth is attributed to the narrow of carrier distribution that most of the carriers can relax into the lowest energy level of the deep localization center with rising in temperature up to 23 K. When further increase of temperature, carriers can have sufficient energy to repopulate the shallow localized states and the linewidth increase linearly. In contrast, the linewidth for half-cavity structure shows no clear downward trend but a continuous increase over the entire temperature range. In addition, the linewidth growth rate of half-cavity structure is around 0.08 meV/K, which is half that of epitaxial layer (0.16 meV/K). All these suggests that the transition behavior of carriers in different localization potentials is prevented due to the cavity effect.

3.2. Carrier dynamics by TRPL

To further investigated the carrier dynamics within QW, TRPL of the epitaxial layer and half-cavity structure were measured at RT. Fig. 4(a) and (b) show the TRPL curves at photon energies of low-energy side (2.7

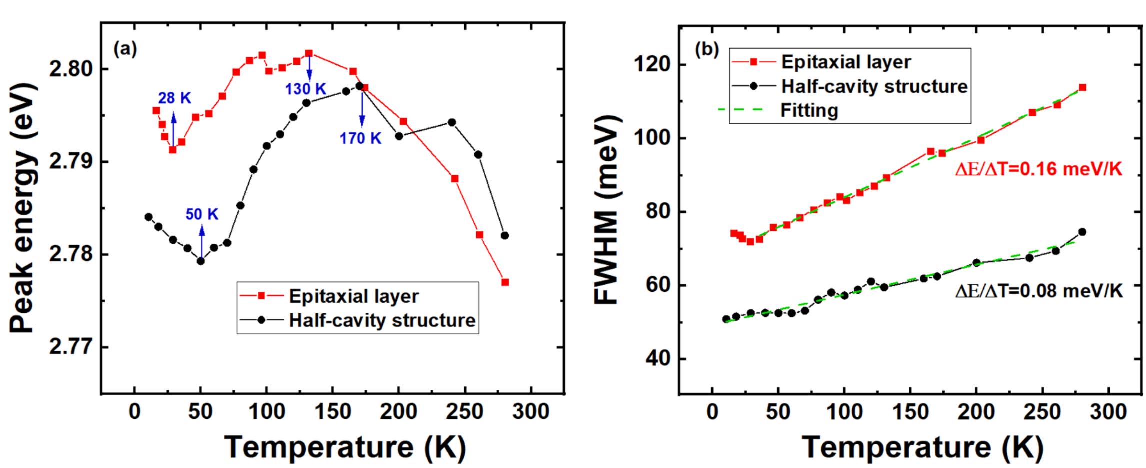

Fig. 3. Temperature dependence of (a) emission peak energies and (b) spectra linewidths (FWHM) measured under different excitation power. The dashed lines are the fitting results.

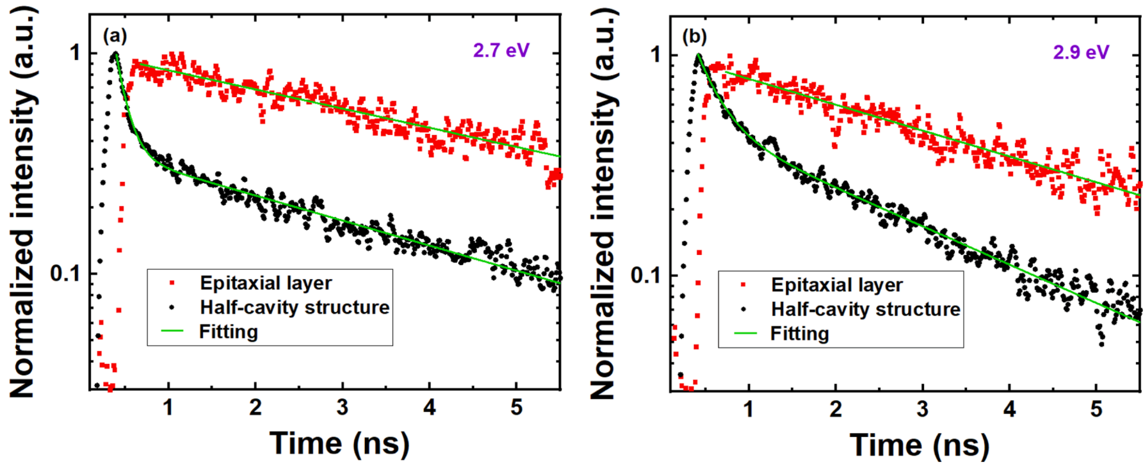

Fig. 4. TRPL curves of epitaxial layer and half-cavity structure at photon energies of (a)2.7 eV and (b)2.9 eV.

eV) and high-energy side (2.9 eV), respectively. The decay curves can be well fitted with a double exponential function [20]:

$$I(t) = B_1 e^{-t/\tau_1} + B_2 e^{-t/\tau_2} \quad (1)$$

where τ_1 and τ_2 represent the carrier lifetime in the fast and slow decay stages, respectively. The obtained fitting results are listed in Table 2.

In general, the carrier lifetime is affected by the carrier recombination, transport and relaxation. From the fitting results, near single exponential decay is observed for epitaxial layer. The decay time of high-energy side is shorter than that of low-energy side, which is mainly due to the carriers transfer from shallow localized states to deep localized states. For half-cavity structure, however, the decay curves exhibit two obvious decay stage (fast component in the initial part and a slow component in the following part) and the carrier lifetime is shortened. The short lifetime indicates that the cavity enhances the radiation recombination rate of carriers. At resonant modes, carriers in localization potential consumes rapidly and the cavity-enhanced recombination can enable more carriers to be captured by localization states. In addition, different from epitaxial layer, the carrier lifetime in initial fast decay at 2.7 eV is shorter than that of 2.9 eV, meaning that there is no transfer process of carriers from high energy side to low energy side. The carrier transfer in different localization potentials is prevented due to the cavity effect, which is consistent with the TDPL result. Thus, both fast and slow decay stage are mainly due to the carrier recombination, and the carrier lifetime can be expressed as [21]

$$\frac{1}{\tau} = \frac{1}{\tau_r} + \frac{1}{\tau_{nr}} \quad (2)$$

where $1/\tau_r$ and $1/\tau_{nr}$ represent the radiative and nonradiative recombination rates, respectively. The two decay stages at different energy sides can be explained as the influence of nonradiative recombination at different carrier densities: For fast decay stage, where the carrier density is high, localizing centers and defect-related nonradiative centers are saturated. Since the deep localized states have the smaller density of states, Auger recombination caused by high carrier density will reduce the carrier lifetime at low-energy side. Thus, the carrier lifetime (τ_1) of 2.7 eV is shorter than that of 2.9 eV. For the slow decay stage, carrier density decreases, and the carrier lifetime (τ_2) is mainly influenced by the defect-related nonradiative centers. The stronger localization effect of deep localized states will result in a longer τ_2 in low-energy side.

Table 2
Carrier lifetimes at two different photon energies.

Photon energy (eV)	Epitaxial layer		–	Half-cavity structure	
	τ_1 (ns)	τ_2 (ns)		τ_1 (ns)	τ_2 (ns)
2.7	5	–		0.13	3.82
2.9	3.7	–		0.26	2.5

3.3. Low threshold lasing of optical pumping VCSEL

Fig. 5 (a) shows the variation of emission spectrum of fabricated VCSEL with increasing the pumping energy. The GaN-based VCSEL was optically pumped at room temperature by a fs impulsive optical excitation at 370 nm, with a repetition rate of 1 kHz and a pulse width of 150 fs. The total thickness of the resonant cavity is about 17λ in optical thickness. As shown in the figure, the transition from spontaneous emission to stimulated emission is obvious. Above the threshold pumping energy, a sharp emission peak appears at 440.9 nm with a linewidth of 0.06 nm. Fig. 5(b) shows the light emission intensity from the VCSEL as a function of the pumping energy. A distinct threshold characteristic was observed at the threshold energy of about 7.4 nJ/pulse corresponding to an energy density of 0.37 mJ/cm^2.

The threshold energy density as a function of the cavity length of the previously reported optical injection VCSELs is summarized in Fig. 6, along with the result reported in this study. A typical threshold energy of optical pumped GaN-based VCSEL with 18λ cavity length was 6.3 mJ/cm^2 [23]. However, the fabricated VCSELs in this study possesses a low threshold energy density and features a narrow linewidth. In addition, the threshold energy density in this study is among the lowest value for optical injection GaN VCSELs. We attributed this improvement mainly to two factors. First is the QW with thin well and barrier. The narrower well and barrier have a higher recombination rate due to the carrier localization effect and weaker QCSE, which can be unambiguously identified by the PL spectra shown in Fig. 2. The second is the thin active region. By using thin active region, a larger gain enhancement factor can be achieved, which can effectively decrease the threshold gain of the VCSEL [26].

Fig. 7 shows the calculated gain enhancement factor as a function of active region thickness. The gain enhancement factor is determined by the spatial overlap of the optical field and the active region, and can be calculated as [26]

$$\Gamma_r = \frac{L\int_{d_a} |E(z)|^2 dz}{d_a \int_L |E(z)|^2 dz} \quad (3)$$

where L, d_a, and E(z) are the cavity length, thickness of the active region, and optical field standing wave pattern, respectively. To explore the optical field distributions, we calculated the standing wave pattern of a 441 nm resonant mode in the VCSELs using the transfer matrix method. In the calculation, we fix the central position of QW, and the thickness of

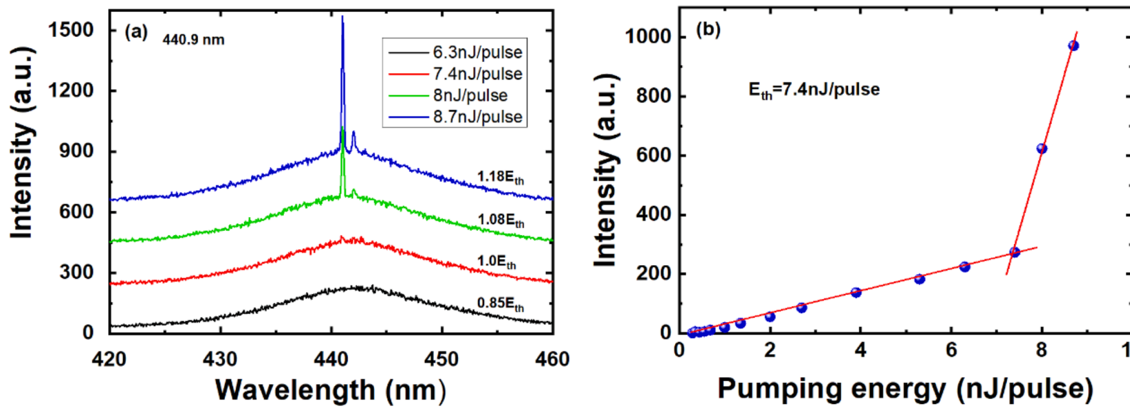

Fig. 5. (a) The variation of emission spectrum with increase of pumping energy. (b) Emission intensity as a function of pumping energy at room temperature.

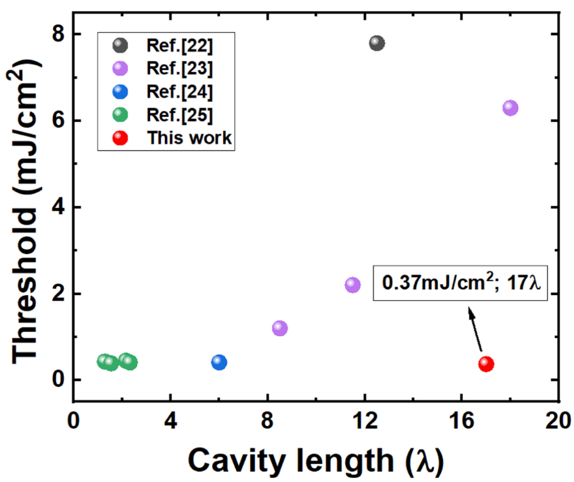

Fig. 6. Threshold energy density of the optical injection GaN-based VCSELs as a function of the cavity length. (See above-mentioned references for further information).

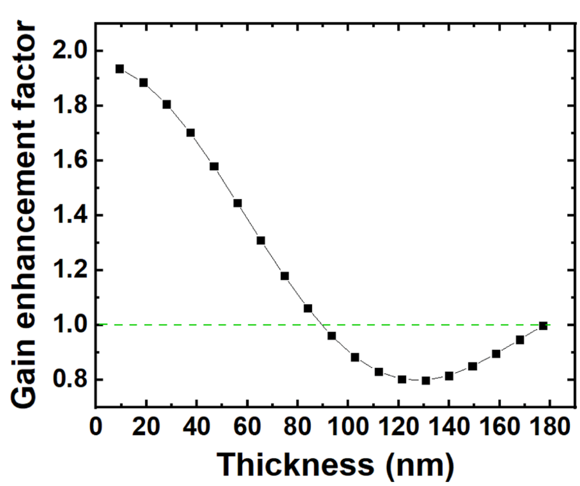

Fig. 7. Gain enhancement factor as a function of active region thickness.

well and barrier are 2.5 nm and 6 nm, respectively. We increase the thickness of active region by increasing the pairs of QW. The numbers of QWs calculated from one pair to twenty-one pairs, corresponding the thickness from 8.5 nm to 178.5 nm. All the parameters used for calculation are consistent with the VCSEL structure used in our experiment. As shown in Fig. 7, when the active region thickness is thin (less than 45 nm), the gain enhancement factor is strongly affected by the relative position of the active region and internal optical field. With further increase of thickness, the variation fluctuation of the gain enhancement factor decreases gradually, and finally approaches 1, which is close to the edge-emitting laser. In this geometry, we can achieve a gain enhancement factor of about 1.8, indicating more effective coupling between the gain medium and internal optical field. The stronger localization effect of thin QW and the strong coupling of QW and optical field contribute to the low threshold lasing of InGaN/GaN QW VCSEL.

Moreover, in addition to the active region thickness, the number of QWs also affect the performance of GaN VCSEL. The increase of well number is conducive to improve the gain of material, which is helpful for achieve high power VCSEL. However, one of the most important issues is the poor hole transportation for GaN material. Due to the relatively low mobility and the large effective mass of the holes in GaN [27], non-uniform carrier distribution within MQW active region will be more significant, resulting in the uneven optical material gain. Some of wells may become absorption wells, thus increasing the lasing threshold. This problem is typically worse in current injection GaN VCSELs since the hole injection is original from p-GaN. Fewer QW numbers can reduce the transparent carrier concentration and final threshold carrier concentration. A. Z. Goharrizi, et al had study the impacts of QW number on the performance of GaN VCSEL by numerical simulations [28]. The simulation results indicate that the DQW GaN-VCSEL has the best performance, which is in good agreement with our experiments. Besides, compared with single QW, DQW can also prevent the leakage of carrier. This work is expected to provide useful reference for realizing low threshold GaN VCSELs by using such an active region structure.

4. Conclusion

In summary, the mechanism of low-threshold lasing of InGaN/GaN DQW VCSELs with thin well and barrier was systematically studied. Carrier dynamics in VCSEL microcavity was investigated by the samples with half-cavity structure using TDPL and TRPL measurements. All these phenomena suggest that, in VCSEL microcavity, the transition of carrier in different QW localization states is inhibited, and the carrier capture efficiency of localization states can be enhanced due to the cavity-enhanced recombination. Since QWs with thin well and barrier show a stronger carrier localization effect, the strong coupling of QW and optical field can contribute to the low-threshold lasing of GaN-based VCSEL. This work can provide considerable insight into the mechanism of low-threshold lasing of InGaN/GaN QW VCSELs.

CRediT authorship contribution statement

Rongbin Xu: Writing – original draft, Investigation, Formal analysis, Data curation. **Keisei Shibata:** Methodology, Investigation, Data curation. **Hidefumi Akiyama:** Writing – review & editing, Formal analysis. **Jiazhe Zhang:** Investigation. **Leiying Ying:** Methodology, Investigation. **Baoping Zhang:** Writing – review & editing, Methodology, Formal analysis, Conceptualization.

Declaration of competing interest

The authors declare that they have no known competing financial interests or personal relationships that could have appeared to influence the work reported in this paper.

Acknowledgments

This work was supported by the National Natural Science Foundation of China (Nos. U21A20493, 62234011).

Data availability

Data will be made available on request.

References

[1] S. P. DenBaars, D. Feezell, K. Kelchner, S. Pimputkar, C. C. Pan, C. C. Yen, S. Tanaka, Y. Zhao, N. Pfaff, R. Farrell, M. Iza, S. Keller, U. Mishra, J. S. Speck, and S. Nakamura., Development of gallium-nitride-based light-emitting diodes (LEDs) and laser diodes for energy-efficient lighting and displays, Acta Mater., vol. 61, no. 3, pp. 945–951, Feb. 2013, 10.1016/j.actamat.2012.10.042.

[2] M. M. Liang, G. E. Weng, J. Y. Zhang, X. M. Cai, X. Q. Lv, L. Y. Ying, B. P. Zhang., Influence of barrier thickness on the structural and optical properties of InGaN/GaN multiple quantum wells, Chin. Phys. B, vol. 23, no. 5, p. 054211, May 2014, 10.1088/1674-1056/23/5/054211.

[3] G. E. Weng, Y. J. Liu, S. Q. Chen, T. Ito, X. B. Hu, C. H. Zhao, J. P. Liu, J. H. Chu, and H. Akiyama., Quantitative study of electron tunneling dynamics in asymmetric coupled InGaN/GaN quantum wells, Appl. Opt., vol. 59, no. 20, p. 6231, Jul. 2020, 10.1364/AO.396999.

[4] M. Hajdel, M. Chlipała, M. Siekacz, H. Turski, P. Wolny, K. Nowakowski-Szkudlarek, Dependence of InGaN quantum well thickness on the nature of optical transitions in LEDs, Materials 15 (1) (Dec. 2021) 237, https://doi.org/10.3390/ma15010237.

[5] Z.C. Feng, L.H. Zhu, T.W. Kuo, C.Y. Wu, H.L. Tsai, B.L. Liu, J.R. Yang, Optical and structural studies of dual wavelength InGaN/GaN tunnel-injection light emitting diodes grown by metalorganic chemical vapor deposition, Thin Solid Films 529 (Feb. 2013) 269–274, https://doi.org/10.1016/j.tsf.2012.05.038.

[6] R.L. Zhou, M. Ikeda, F. Zhang, J.P. Liu, S.M. Zhang, A.Q. Tian, P.Y. Wen, D.Y. Li, L. Q. Zhang, H. Yang, Total-InGaN-thickness dependent Shockley-Read-Hall recombination lifetime in InGaN quantum wells, J. Appl. Phys. 127 (1) (Jan. 2020) 013103, https://doi.org/10.1063/1.5131716.

[7] Y.H. Cho, G.H. Gainer, A.J. Fischer, J.J. Song, S. Keller, U.K. Mishra, S.P. DenBaars, 'S-shaped' temperature-dependent emission shift and carrier dynamics in InGaN/GaN multiple quantum wells, Appl. Phys. Lett. 73 (10) (Sep. 1998) 1370–1372, https://doi.org/10.1063/1.122164.

[8] T. Wang et al., "Investigation of the Optical Properties in InGaN/GaN Quantum Well Structure," phys. stat. sol. (b), vol. 216, pp. 279, Nov. 1999, 10.1002/(SICI)1521-3951(199911)216:1<279::AID-PSSB279>3.0.CO;2-0.

[9] Y. Y. Zhang, X. H. Zhang, K. H. Li, Y. F. Cheung, C. Feng, and H. W. Choi, "Advances in III-nitride semiconductor microdisk lasers," phys. status solidi (a), vol. 212, no. 5, pp. 960–973, Mar. 2015, 10.1002/pssa.201431745.

[10] G.Y. Zhu, F.F. Qin, X. Li, Y. Sun, F. Gao, M.F. Tian, B.J. Ji, Y.J. Wang, Research progress of gallium nitride microdisk cavity laser, Front. Mater. 9 (Apr. 2022) 845885, https://doi.org/10.3389/fmats.2022.845885.

[11] W. Chen, M. Feng, Y. Tang, J. Wang, J. Liu, Q. Sun, X. Gao, Y. Wang, H. Yang, GaN-based resonant-cavity light-emitting diodes grown on Si, Nanomaterials 12 (1) (Dec. 2021) 134, https://doi.org/10.3390/nano12010134.

[12] C.J. Wang, Y. Ke, G.Y. Shiu, Y.Y. Chen, Y.S. Lin, H. Chen, C.F. Lin, InGaN resonant-cavity light-emitting diodes with porous and dielectric reflectors, Appl. Sci. 11 (1) (Dec. 2020) 8, https://doi.org/10.3390/app11010008.

[13] M. Kuramoto, S. Kobayashi, T. Akagi, K. Tazawa, K. Tanaka, T. Saito, T. Takeuchi, High-power GaN-based vertical-cavity surface-emitting lasers with AlInN/GaN distributed Bragg reflectors, Appl. Sci. 9 (3) (Jan. 2019) 416, https://doi.org/10.3390/app9030416.

[14] H.C. Yu, Z.W. Zheng, Y. Mei, R.B. Xu, J.P. Liu, H. Yang, B.P. Zhang, T.C. Lu, H. C. Kuo, Progress and prospects of GaN-based VCSEL from near UV to green emission, Prog. Quant. Electron. 57 (Jan. 2018) 1–19, https://doi.org/10.1016/j.pquantelec.2018.02.001.

[15] T. Hamaguchi, GaN-based VCSELs with a monolithic curved mirror, "GaN-based VCSELs with a monolithic curved mirror: Challenges and prospects, Photonics 10 (4) (Apr. 2023) 470, https://doi.org/10.3390/photonics10040470.

[16] E.F. Schubert, Y.H. Wang, A.Y. Cho, L.W. Tu, G.J. Zydzik, Resonant cavity light-emitting diode, Appl. Phys. Lett. 60 (8) (Feb. 1992) 921–923, https://doi.org/10.1063/1.106489.

[17] W.W. Chow, H. Amano, T. Takeuchi, J. Han, Quantum-well width dependence of threshold current density in InGaN lasers, Appl. Phys. Lett. 75 (Jul. 1999) 244–246, https://doi.org/10.1063/1.124336.

[18] R.A. Abdullah, K. Ibrahim, Simulation of high power with low threshold current of violet InGaN laser diode based on optimization of its active region, Optoelectron. Adv. Mater. - Rapid Commun. 4 (3) (Mar. 2010) 287–290.

[19] S. W. Feng, Y. C. Cheng, Y. Y. Chung, C. C. Yang, Y. S. Lin, C. Hsu, K. J. Ma, and J. I. Chyi., "Impact of localized states on the recombination dynamics in InGaN/GaN quantum well structures," J. Appl. Phys., vol. 92, no. 8, pp. 4441–4448, Oct. 2002, 10.1063/1.1506393.

[20] L. Liu, L. Wang, N. Liu, W. Yang, D. Li, W. Chen, Z. Chuan Feng, Y.C. Lee, I. Ferguson, X. Hul, Investigation of the light emission properties and carrier dynamics in dual-wavelength InGaN/GaN multiple-quantum well light emitting diodes, J. Appl. Phys. 112 (8) (2012) Oct, https://doi.org/10.1063/1.4759373.

[21] L. Wang, Y. Xing, Z. Hao, and Y. Luo, "Study on carrier lifetimes in InGaN multi-quantum well with different barriers by time-resolved photoluminescence," phys. status solidi (b), vol. 252, no. 5, pp. 956–960, Dec. 2014, 10.1002/pssb.201451511.

[22] J.Y. Zhang, L.E. Cai, B.P. Zhang, S.Q. Li, F. Lin, J.Z. Shang, D.X. Wang, K.C. Lin, J. Z. Yu, Q.M. Wang, Low threshold lasing of GaN-based vertical cavity surface emitting lasers with an asymmetric coupled quantum well active region, Appl. Phys. Lett. 93 (19) (2008) Nov, https://doi.org/10.1063/1.3030876.

[23] W. J. Liu, X. L. Hu, L. Y. Ying, S. Q. Chen, J. Y. Zhang, H. Akiyama, Z. P. Cai, and B. P. Zhang, "On the importance of cavity-length and heat dissipation in GaN-based vertical-cavity surface-emitting lasers," Sci. Rep., vol. 5, no. 1, Apr. 2015, 10.1038/srep09600.

[24] J.Z. Wu, H. Long, X.L. Shi, L.Y. Ying, Z.W. Zheng, B.P. Zhang, Reduction of lasing threshold of GaN-based vertical-cavity surface-emitting lasers by using short cavity lengths, IEEE Trans. Electron Devices 65 (6) (Jun. 2018) 2504–2508, https://doi.org/10.1109/TED.2018.2825992.

[25] Y. Mei, T.R. Yang, W. Ou, Z.M. Zheng, H. Long, L.Y. Ying, B.P. Zhang, Low-threshold wavelength-tunable ultraviolet vertical-cavity surface-emitting lasers from 376 to 409 nm, Fundam. Res. 1 (6) (Nov. 2021) 684–690, https://doi.org/10.1016/j.fmre.2021.11.001.

[26] R. Michalzik, Fundamentals, Technology and Applications of Vertical Cavity Surface-Emitting Lasers. Berlin, Germany: Springer, 2013, pp. 27–30.

[27] T.T. Mnatsakanov, M.E. Levinshtein, L.I. Pomortseva, S.N. Yurkov, G.S. Simin, M. A. Khan, Carrier mobility model for GaN, Solid State Electron. 47 (1) (Jan. 2003) 111–115, https://doi.org/10.1016/S0038-1101(02)00256-3.

[28] A.Z. Goharrizi, G. Alahyarizadeh, Z. Hassan, H.A. Hassan, Study on effect of quantum well number on performance characteristics of GaN-based vertical cavity surface emitting laser, Physica E 50 (6) (Feb. 2013) 61–66, https://doi.org/10.1016/j.physe.2013.02.019.